IEEE Access
Multidisciplinary | Rapid Review | Open Access Journal

Received January 6, 2021, accepted January 15, 2021, date of publication January 18, 2021, date of current version January 27, 2021.

Digital Object Identifier 10.1109/ACCESS.2021.3052689

Fano Resonance Among Magnetic Coils for Midrange Position Sensing Capability

TAEHWA LEE[1], (Member, IEEE), DANIEL HASHEMI[1], KENICHI YATSUGI[2], MICHIO YASUNISHI[3], HIROSHI YOSHIMOTO[3], AND HIDEO IIZUKA[1], (Member, IEEE)

[1]Toyota Research Institute of North America, Toyota Motor North America, Ann Arbor, MI 48105, USA
[2]Toyota Central Research and Development Laboratories, Nagakute 480-1192, Japan
[3]Toyota Motor Corporation, Toyota 471-8571, Japan

Corresponding author: Hideo Iizuka (hideo.iizuka@toyota.com)

ABSTRACT A magnetically coupled three-coil system to have one transmitting and two receiving coils is considered. We show that the position of the transmitting coil can be estimated from the ratio of received wave amplitudes and its angular derivative when the two receiving coils are strongly coupled to each other and each of the receiving coils is weakly coupled to the transmitting coil, i.e., a Fano resonance phenomenon. A coupled mode theory is developed to elucidate the midrange position sensing mechanism, where the ratio of received wave amplitudes is inversely proportional to the ratio of the coupling strengths of each receiving coil to the transmitting coil at the intrinsic resonance frequency of the receiving coils.

INDEX TERMS Electromagnetics, electromagnetic coupling, magnetic resonance, coils, coupled mode analysis.

I. INTRODUCTION

Midrange coupling via magnetic fields in the kilohertz-megahertz range has been extensively explored in wireless power transfer [1]–[16], and found various application scenarios in consumer electronics [17], [18], electric vehicles [19]–[22], and medical implants [23]–[25]. Estimating the position of a magnetic coil in the midrange is of great importance in wireless power transfer systems for improving system performances [26]. In electromagnetic compatibility, magnetic noise sources need to be found and suppressed [27], [28]. Particularly, in the development of electric vehicles, a dominant noise source, such as common mode noise generated from a power converter during switching operation, must be identified [29].

Fano resonance occurs from the interference between direct and resonance-assisted indirect pathways, and exhibits an asymmetric line shape in the frequency response [30]–[33]. Recently, in the far-field regime, an angle estimation technique of an incoming wave in a subwavelength size has been studied in optics [34] and acoustics [35], where two waveguides or resonators are strongly coupled in the receiver, and the ratio of the two received wave amplitudes estimates an angle of the incoming wave.

The associate editor coordinating the review of this manuscript and approving it for publication was Wei Xu.

Inspired by the far-field angle sensing technique, here we extend the analogy to the kilohertz-megahertz range where no phase rotation occurs between a transmitter and a receiver. We show that in a magnetically-coupled system consisting of one transmitting and two receiving coils, both the angle and the distance of the transmitting coil can be estimated from the ratio of received wave amplitudes and its angular derivative when the two receiving coils are strongly coupled to each other and each of the receiving coils is weakly coupled to the transmitting coil. Our result indicates the possibility to estimate the position of a noise source with a pair of coils, assuming the transmitting coil as a noise source. A coupled mode theory is developed to elucidate the midrange position sensing mechanism.

In [26], a receiving coil was moved parallel above an array of transmitting coils with each having a switch, and the position of the receiving coil was estimated from the comparison of a measured input impedance at each transmitter to numerical data sets. In that system, the distance between the receiving coil and the array of transmitting coils was fixed and a known parameter. Whereas our system is able to estimate both the distance and the angle of a transmitting coil. In [36]–[38], wireless power transfer systems having multiple-receivers have been reported, but angle sensing capability in the midrange magnetic coupling scheme has not been reported.

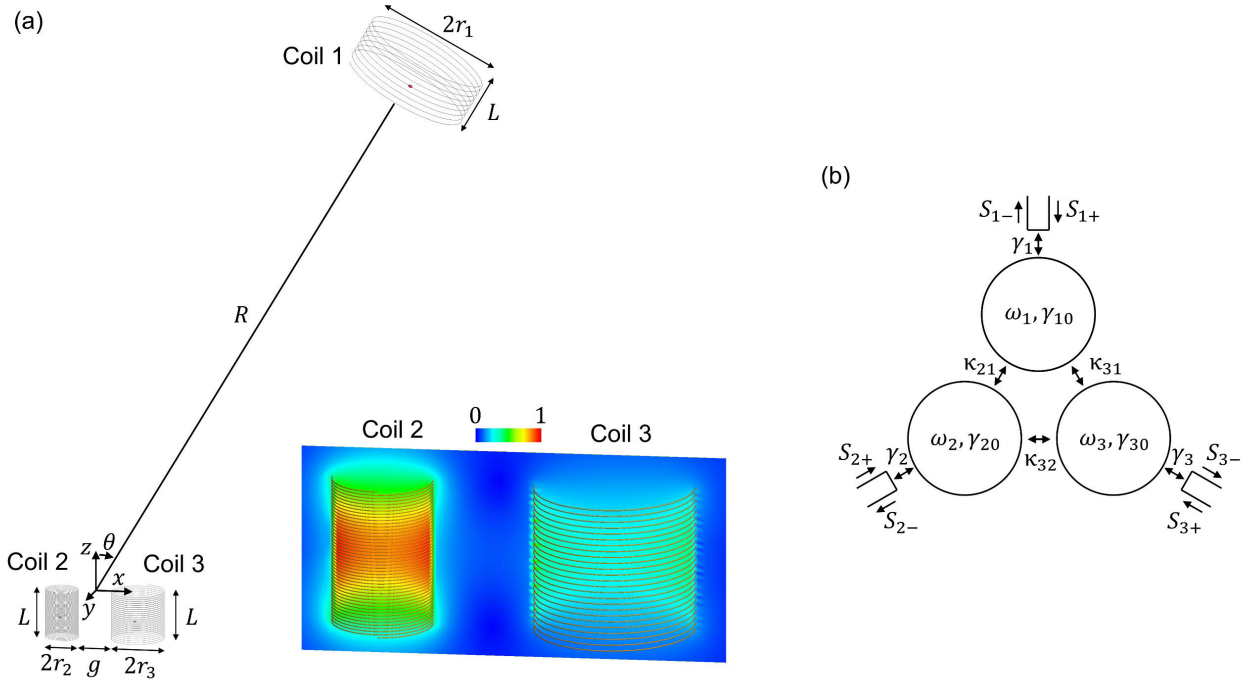

FIGURE 1. (a) Geometry of a three-coil system consisting of one transmitting coil (coil 1) and two receiving coils (coils 2 and 3). (coil radii: $r_1 = 20$ *cm*, $r_2 = 5$ *cm*, $r_3 = 8$ *cm*, coil length: $L = 15$ *cm*, gap size: $g = 10$ *cm*, number of wire turns: $N_1 = 8.42$, $N_2 = 46$, $N_3 = 24.9$) These values are used throughout the paper unless mentioned, and the position (R, θ) of coil 1 is varied. The inset shows the magnetic field distribution of coils 2 and 3 at a frequency of 10 *MHz* when coil 1 is placed at $R = 2$ *m* and $\theta = 30°$. (b) Semi-analytic model of Fig. 1(a).

This article is organized as follows. In Section II, the geometry of a three-coil system is presented and a coupled mode theory is developed to elucidate how the three coils are coupled. In Section III, numerical results of the system performance are presented, revealing that both the angle and the distance of a transmitting coil are uniquely determined in a Fano resonance phenomenon. In addition, the effects of conductor loss of coils and the presence of a ground plane near the receiving coils are investigated, verifying that our system performance is robust due to the use of the ratio of received wave amplitudes. This article is concluded in Section IV.

II. GEOMETRY AND THEORY

A. GEOMETRY

A three-coil system to have one transmitting coil (coil 1) and two receiving coils (coils 2 and 3) is considered, as shown in Fig. 1(a). Coils 1, 2, and 3 have different radii $r_1 = 20$ *cm*, $r_2 = 5$ *cm*, and $r_3 = 8$ *cm* while having the same resonance frequency of 10 *MHz*, which are obtained by different numbers of wire turns $N_1 = 8.42$, $N_2 = 46$, and $N_3 = 24.9$, respectively, in a common coil length $L = 15$ *cm*. The three coils have the same winding direction and a wire radius of 0.5 *mm* with their axes being parallel to the zx plane. Coils 2 and 3 are placed with a small gap distance of $g = 10$ *cm* and thus they are strongly coupled to each other by magnetic fields. Coil 1 is placed at position (R, θ) far away from the pair of coils 2 and 3, and is weakly coupled to each of coils 2 and 3 by magnetic fields, where R is the distance from the coil pair and θ is the angle from the z axis in the zx plane [θ and x have the same sign]. The origin of the coordinate system lies at the middle of the gap between coils 2 and 3 with the top end of each coil on the x axis. The axis of coil 1 directs to the origin of the coordinate system. This is a Fano resonance phenomenon that can provide a unique ratio of received wave amplitudes in the receiving coils, enabling position sensing of coil 1. Below we will refer to scattering parameters S_{ji} (coils i to j) or voltages V_j (coil j) for evaluating characteristics of the system of Fig. 1.

B. THEORY

To elucidate the Fano resonance phenomenon, a coupled mode theory is developed, where a semi-analytic model consists of three coupled resonators, as shown in Fig. 1(b). It is assumed that the system is reciprocal, and far-field radiation leakage from each coil is negligibly small. The $e^{i\omega t}$ convention is used. Referring [39], [40], with an incident wave at port 1, the system dynamics is given by:

$$\frac{da_1}{dt} = (i\omega_1 - \gamma_{10} - \gamma_1)\, a_1 + i\kappa_{21} a_2 + i\kappa_{31} a_3 + \sqrt{2\gamma_1} S_{1+}, \tag{1a}$$

$$\frac{da_2}{dt} = (i\omega_2 - \gamma_{20} - \gamma_2)\, a_2 + i\kappa_{21} a_1 + i\kappa_{32} a_3, \tag{1b}$$

$$\frac{da_3}{dt} = (i\omega_3 - \gamma_{30} - \gamma_3)\, a_3 + i\kappa_{31} a_1 + i\kappa_{32} a_2, \quad (1c)$$

$$S_{1-} = -S_{1+} + \sqrt{2\gamma_1} a_1, \quad (1d)$$

$$S_{2-} = \sqrt{2\gamma_2} a_2, \quad (1e)$$

$$S_{3-} = \sqrt{2\gamma_3} a_3, \quad (1f)$$

where a_j is the mode amplitude of resonator j and is normalized so that $|a_j|^2$ represents the mode energy. ω_j and γ_{j0} are the resonance frequency and the intrinsic loss rate of resonator j. κ_{ji} is the coupling rate between resonators i and j. S_{j+} and S_{j-} are the input and output wave amplitudes at port j. γ_j is the coupling rate between resonator j and port j. t is time. In the frequency domain, Eqs. (1a)-(1c) are written as:

$$\begin{pmatrix} A_{11} & -i\kappa_{21} & -i\kappa_{31} \\ -i\kappa_{21} & A_{22} & -i\kappa_{32} \\ -i\kappa_{31} & -i\kappa_{32} & A_{33} \end{pmatrix} \begin{pmatrix} a_1 \\ a_2 \\ a_3 \end{pmatrix} = \begin{pmatrix} \sqrt{2\gamma_1} S_{1+} \\ 0 \\ 0 \end{pmatrix}. \quad (2)$$

where $A_{jj} = i(\omega - \omega_j) + \gamma_{j0} + \gamma_j$. From Eqs. (2) and (1d)-(1f), the output wave amplitudes at ports 2 and 3 with respect to the incident wave are given by:

$$S_{21} = \frac{S_{2-}}{S_{1+}} = \frac{2\sqrt{\gamma_1\gamma_2}\,\{i\kappa_{21}\,[i(\omega - \omega_3) + \gamma_{30} + \gamma_3] - \kappa_{31}\kappa_{32}\}}{det\left(\overleftrightarrow{A}\right)}, \quad (3a)$$

$$S_{31} = \frac{S_{3-}}{S_{1+}} = \frac{2\sqrt{\gamma_1\gamma_3}\,\{i\kappa_{31}\,[i(\omega - \omega_2) + \gamma_{20} + \gamma_2] - \kappa_{21}\kappa_{32}\}}{det\left(\overleftrightarrow{A}\right)}, \quad (3b)$$

where $det\left(\overleftrightarrow{A}\right)$ is the determinant of the matrix in the left-hand side of Eq. (2). From Eqs. (3a) and (3b), the ratio of the output amplitudes of ports 2 to 3 is led:

$$\frac{S_{21}}{S_{31}} = \frac{S_{2-}}{S_{3-}} = \sqrt{\frac{\gamma_2}{\gamma_3}} \frac{i\kappa_{21}\,[i(\omega - \omega_3) + \gamma_{30} + \gamma_3] - \kappa_{31}\kappa_{32}}{i\kappa_{31}\,[i(\omega - \omega_2) + \gamma_{20} + \gamma_2] - \kappa_{21}\kappa_{32}}. \quad (4)$$

Eqs. (3a), (3b), and (4) are used for obtaining semi-analytical results throughout the paper. When two resonators 2 and 3 are strongly coupled $\kappa_{32} \gg (\kappa_{21}, \kappa_{31}, \gamma_2, \gamma_3)$, and have the same resonance frequencies $\omega_2 = \omega_3 = \omega_0$ in the lossless case $\gamma_{20} = \gamma_{30} = 0$, Eq. (4) at $\omega = \omega_0$ is approximately written as:

$$\frac{S_{21}}{S_{31}} \approx \sqrt{\frac{\gamma_2}{\gamma_3}} \frac{\kappa_{31}}{\kappa_{21}}. \quad (5)$$

Eq. (5) reveals that the ratio of the wave amplitudes S_{21}/S_{31} at the frequency $\omega = \omega_0$ is inversely proportional to the ratio of the coupling strengths of each of resonators 2 and 3 to resonator 1, i.e., one receiving coil (coil 2 or 3) having weaker coupling to coil 1 has larger wave amplitude comparing with the other receiving coil. The coupling rates are dependent on the position of coil 1, i.e., $\kappa_{21} = \kappa_{21}(R, \theta)$, $\kappa_{31} = \kappa_{31}(R, \theta)$, while γ_2, γ_3 are independent of the coil 1 position. Below we will show that the position of coil 1 can be uniquely determined by the ratio S_{21}/S_{31} and the derivative to angle $\frac{d}{d\theta}(S_{21}/S_{31})$.

III. RESULTS

A. SYSTEM PERFORMANCE

The system of Fig. 1(a) is numerically investigated by the method of moment simulator, Altair FEKO [41] since Altair FEKO showed good agreement between numerical and experimental results in magnetic resonance coupling between coils around 10 *MHz* [14]. In the system of Fig. 1(a), a voltage of 1V is applied at the port of coil 1, and voltages are numerically obtained at each port of coils 2 and 3 by Altair FEKO. The lossless case is assumed for the sake of simplicity unless mentioned. Fig. 2(a) shows the frequency responses of $|S_{21}|$ (blue line and symbols) and $|S_{31}|$ (pink line and symbols) in the system of Fig. 1(a) when coil 1 is placed at $R = 2$ *m* and $\theta = 30^{\circ}$. Figure 2(b)-(d) show the spectra of transmission coefficients between two coils when one of the three coils is taken out, e.g., coil 3 is taken out in the system for Fig. 2(b). It is noted that $\left|S_{ji}^0\right|$ and $|S_{ji}|$ represent scattering parameters in the two-coil and the three-coil systems, respectively. In each of two-coil systems consisting of coils 1 and 2 [Fig. 2(b)], and consisting of coils 1 and 3 [Fig. 2(c)], a single resonance peak is observed at 10 *MHz*, and the coupling between coils 1 and 2 is weaker than the coupling between coil 1 and coil 3 ($|S_{21}^0| < |S_{31}^0|$ for the peaks) when $R = 2$ *m* and $\theta = 30°$ for coil 1. On the other hand, in Fig. 2(d), coils 2 and 3 are strongly coupled and thus the frequency split occurs with two peaks at 10 ± 0.3 *MHz*. In the three-coil system, the spectra of $|S_{21}|$ (blue line) and $|S_{31}|$ (pink line) have the first and the second peaks around 10 ± 0.3 *MHz*[Fig. 2(a)]. An important observation is that coil 2 has larger wave amplitude than coil 3 (pink line) at 10 *MHz*, as the coupled mode theory revealed [Eq. (5)]. This is seen in the magnetic field distribution [inset of Fig. 1(a)], where coil 2 has stronger magnetic fields comparing with coil 3. The parameters for the coupled mode theory have been retrieved from the numerical results of $|S_{21}^0|$, $|S_{31}^0|$ and $|S_{32}^0|$ in the two-coil systems [Fig. 2(b)–(d)], and presented in the caption of Fig. 2. The coupled mode theory (symbols) with the retrieved parameters excellently captures the Fano resonance spectra of the three-coil system observed in the numerical results [solid lines in Fig. 2(a)].

Next the dependency of the ratio $|S_{21}/S_{31}|$ on the position (R, θ) of coil 1 is investigated. Figure 3(a) shows the ratio $|S_{21}/S_{31}|$ as a function of angle θ for $R = 0.5$ *m* (brown curve), $R = 1$ *m* (blue curve), $R = 2$ *m* (pink curve), and $R = 3$ *m* (green curve) at 10 *MHz*. It is seen that the ratio $|S_{21}/S_{31}|$ monotonically increases as angle θ increases in a range of $\pm 80°$. In addition, the slope of the ratio, which is the derivative to angle $\frac{d}{d\theta}|S_{21}/S_{31}|$, becomes steep as coil 1 gets closer to the pair of coils 2 and 3. Therefore, the position

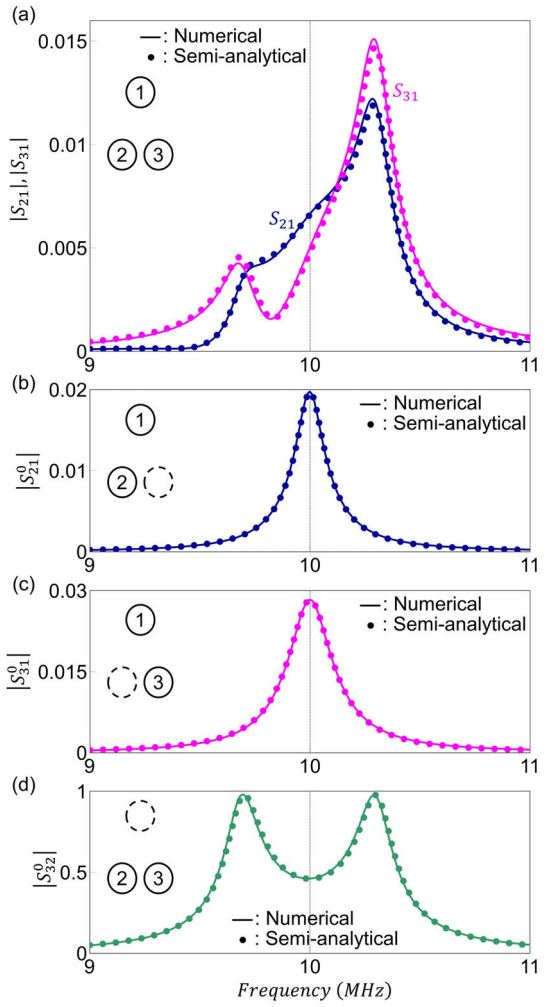

FIGURE 2. (a) Spectra of $|S_{21}|$ (blue line and symbols) and $|S_{31}|$ (pink line and symbols) in the system of Fig. 1(a) when coil 1 is placed at $R = 2$ *m* and $\theta = 30°$. The solid lines and symbols represent the numerical results obtained by Altair FEKO and the semi-analytical results obtained by the coupled mode theory [Eqs. (3a) and (3b)]. ($\kappa_{21} = 1.07$ *kHz*, $\kappa_{31} = 1.93$ *kHz*, $\kappa_{32} = 308$ *kHz*, $\gamma_1 = 198$ *kHz*, $\gamma_2 = 60$ *kHz*, $\gamma_3 = 94$ *kHz*, $\omega_1 = \omega_2 = \omega_3 = 10$ *MHz*, $\gamma_{10} = \gamma_{20} = \gamma_{30} = 0$) (b)-(d) Spectra of $\left|S^0_{ji}\right|$ in the system of Fig. 1(a) where coil k of the three coils (i, j, and k) is taken out. [$k = 3$ for (b), $k = 2$ for (c), $k = 1$ for (d)].

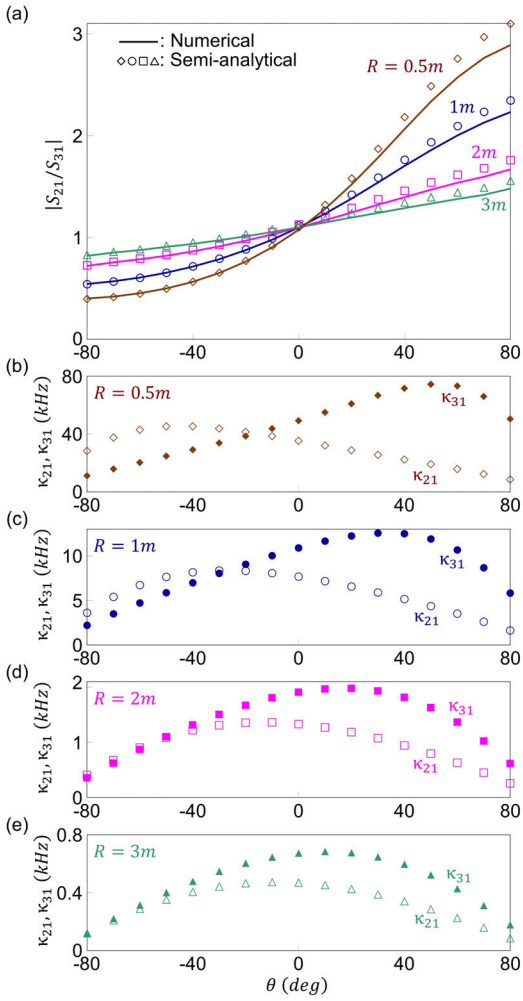

FIGURE 3. (a) Ratio $|S_{21}/S_{31}|$ of received wave amplitudes as a function of the position (R, θ) of coil 1 at 10 *MHz*. The solid lines and symbols represent the numerical results obtained by Altair FEKO and the semi-analytical results obtained by the coupled mode theory [Eq. (4)]. (brown line and diamonds: $R = 0.5$ *m*, blue line and circles: $R = 1$ *m*, pink line and squares: $R = 2$ *m*, green line and triangles: $R = 3$ *m*) (b)-(d) Coupling rates κ_{21} (open symbols) and κ_{31} (filled symbols) as a function of angle θ at $R = 0.5$ *m* for (b), $R = 1$ *m* for (c), $R = 2$ *m* for (d), and $R = 3$ *m* for (e).

of coil 1 is determined by the ratio of the received wave amplitudes $|S_{21}/S_{31}|$ and its derivative $\frac{d}{d\theta}|S_{21}/S_{31}|$, unlike the far-field sensing [35] where the angle of an incident wave was determined without distance information. Practically, for example, the mechanical rotation of the pair of coils 2 and 3 by a few tens of degrees may provide $\frac{d}{d\theta}|S_{21}/S_{31}|$. The semi-analytical results (symbols) obtained from Eq. (4) agree well with the numerical results (curves) obtained by using Altair FEKO. The discrepancy comes from the assumption of the coupled mode theory having the first derivative in time. For example, in the two-coil system of Fig. 2(d), the coupled mode theory shows the frequency split of $\omega_3 \pm \kappa_{32}$ (symbols), and a good approximation with the numerical result (curve) in this coupling regime. On the other hand, the frequency split in the numerical result is not exactly symmetric, and the asymmetricity is observed for much stronger coupling with narrower gap distance between the coils.

The dependency of $|S_{21}/S_{31}|$ on distance R can be understood from coupling rates between coils 1 and 2 and between coils 1 and 3. In the absence of either coil 2 or 3, coupling rates $\kappa_{21}(R, \theta), \kappa_{31}(R, \theta)$ have the form of $\kappa_{j1} = \sqrt{\gamma_1 \gamma_j}\left(1 - \sqrt{1 - \left|S^0_{j1}\right|^2}\right) / \left|S^0_{j1}\right|$ from Eqs. (3a),(3b), and are plotted in Fig. 3(b)-(e), where $\left|S^0_{j1}\right|$ is numerically obtained in the two-coil system between coils 1 and j, i.e., κ_{j1} is the retrieved parameters. Note that $\kappa_{j1} \approx \sqrt{\gamma_1 \gamma_j}\left|S^0_{j1}\right|/2$ when $\left|S^0_{j1}\right| \ll 1$. As coil 1 gets closer to the pair of coils 2 and 3,

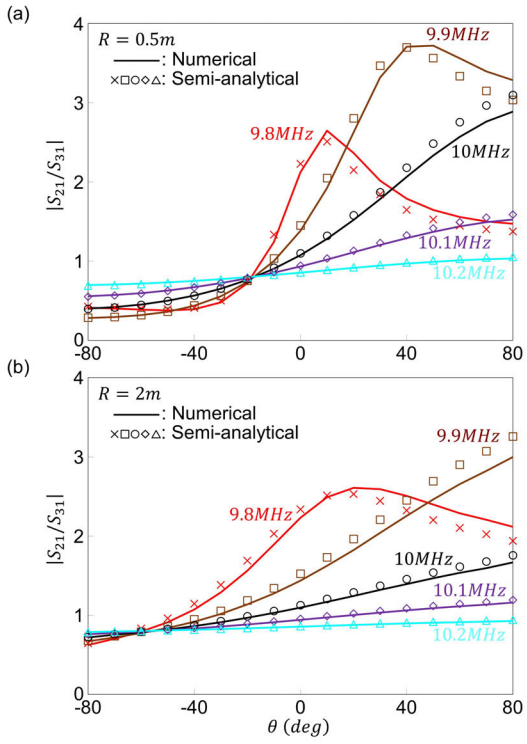

FIGURE 4. (a) Ratio $|S_{21}/S_{31}|$ of received wave amplitudes as a function of the position (R, θ) of coil 1 for frequencies around the resonance at (a) $R = 0.5$ *m* and (b) $R = 2$ *m*, respectively. The solid lines and symbols represent the numerical results obtained by Altair FEKO and the semi-analytical results obtained by the coupled mode theory [Eq. (4)]. (red lines and crosses: 9.8 *MHz*, brown lines and squares: 9.9 *MHz*, black lines and circles: 10 *MHz*, purple lines and diamonds: 10.1 *MHz*, cyan lines and triangles: 10.2 *MHz*).

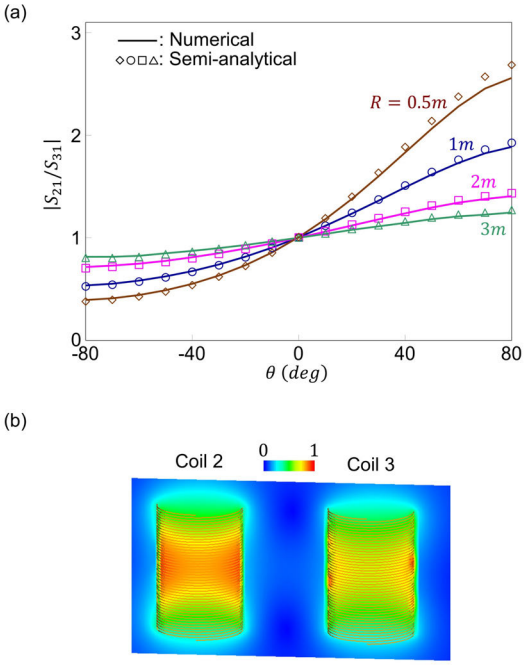

FIGURE 5. (a) Ratio $|S_{21}/S_{31}|$ of received wave amplitudes in the system of Fig. 1(a), where coils 2 and 3 are identical (coil radius: $r_2 = r_3 = 5$ *cm*, number of wire turns: $N_2 = N_3 = 46$), as a function of the position (R, θ) of coil 1 at 10 *MHz*. Other geometrical parameters are the same as those in the caption of Fig. 1. The solid lines and symbols represent the numerical results obtained by Altair FEKO and the semi-analytical results obtained by the coupled mode theory [Eq. (4)]. (brown line and diamonds: $R = 0.5$ *m*, blue line and circles: $R = 1$ *m*, pink line and squares: $R = 2$ *m*, green line and triangles: $R = 3$ *m*) (b) Magnetic field distribution of coils 2 and 3 at 10 *MHz* when coil 1 is placed at $R = 2$ *m* and $\theta = 30°$.

the difference between κ_{21} (open symbols) and κ_{31} (filled symbols) is pronounced, resulting in large $\frac{d}{d\theta}|S_{21}/S_{31}|$.

Other frequencies around the resonance can be used for the position sensing mechanism. Figure 4(a) and 4(b) show the ratio $|S_{21}/S_{31}|$ as a function of angle θ for frequencies of 9.8 *MHz* to 10.2 *MHz* at distances of $R = 0.5$ *m* and $R = 2$ *m*, respectively. For example, selecting a frequency of 9.9 *MHz* (brown line and squares) provides higher sensitivity (steeper slope of $|S_{21}/S_{31}|$) at $R = 2$ *m* [Fig. 4(b)] but a non-monotonic characteristic of $|S_{21}/S_{31}|$ with respect to angle θ at $R = 0.5$ *m* [Fig. 4(a)] while the resonance frequency of 10 *MHz* exhibits a monotonic increase of $|S_{21}/S_{31}|$ to angle θ for both distances of $R = 0.5$ *m* and 2 *m* (black lines and circles). Practically, frequencies may be selected to adjust slopes in the angular sensitivity and satisfy requirements of distance R and angle θ ranges for a concrete application scenario. It is noted that the result of Fig. 4 implies fabrication tolerance of coils on the position sensing performance.

Different radii for the two receiving coils have been used to enhance the asymmetry in coupling rates, which is not necessary for the position sensing mechanism. The pair of identical receiving coils exhibits less sensitivity of the ratio $|S_{21}/S_{31}|$ to angle θ [Fig. 5(a)], comparing with the different radii case [Fig. 3(a)]. The less sensitivity is observed in Fig. 5(b) that coils 2 and 3 have less asymmetry in the magnetic field distribution, comparing with the inset of Fig. 1.

B. INCLINED TRANSMITTING COIL

The axis of coil 1 has been directed to the origin of the coordinate system in Fig. 1. The position sensing performance is investigated when the axis of coil 1 is inclined by angle φ in the zx plane, as shown in Fig. 6(a). The received wave amplitudes $|S_{21}|$ and $|S_{31}|$ are numerically obtained and shown in Fig. 6(b)-(i). As the angle of the coil 1 axis is varied as $\varphi = 15°$ [Fig. 6(b),(c)], 30° [Fig. 6(d),(e)], 45° [Fig. 6(f),(g)], and 60° [Fig. 6(h),(i)], both wave amplitudes $|S_{21}|$ (thick purple dashed-dotted lines) and $|S_{31}|$ (thick cyan dashed-dotted lines) are similarly deviated in Fig. 6(c),(e),(g),(i), as a typical behavior at a distance $R = 2$ *m*. Utilizing the ratio $|S_{21}/S_{31}|$ allows us to maintain the position sensing capability [thick dashed-dotted lines in Fig. 6(b),(d),(f),(h)], where various curves are observed in the ratio $|S_{21}/S_{31}|$ as a function of the position (R, θ). It would be interesting to explore the possibility to estimate (R, θ, φ) of coil 1 by introducing sophisticated algorithms.

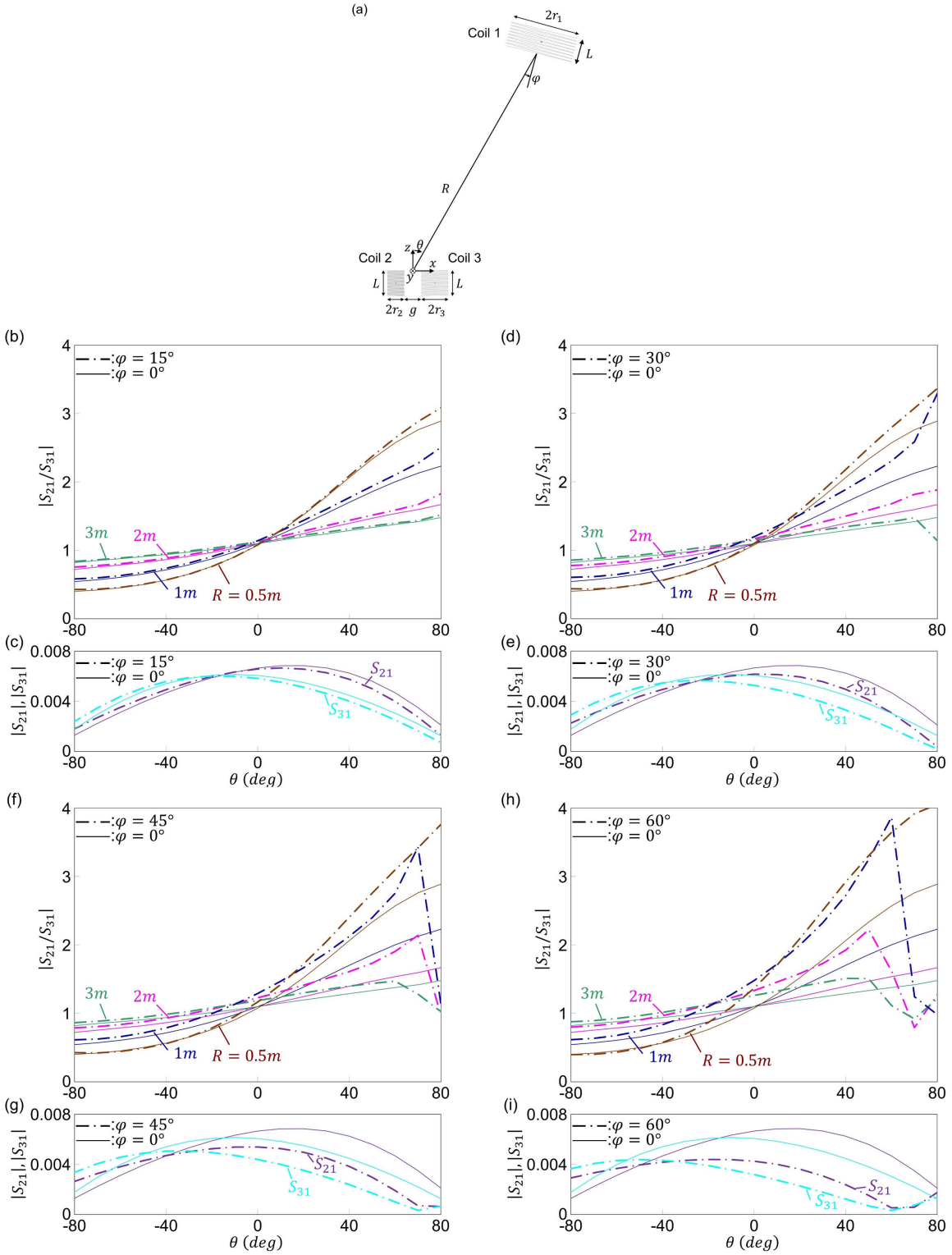

FIGURE 6. (a) Geometry of the system of Fig. 1(a), where the axis of coil 1 is inclined by angle $\varphi = 15°$ (b),(c), 30° (d),(e), 45° (f),(g), and 60° (h),(i). (b)-(i) Position sensing performance (b),(d),(f),(h) at 10 *MHz*. (brown lines: $R = 0.5$ *m*, blue lines: $R = 1$ *m*, pink lines: $R = 2$ *m*, green lines: $R = 3$ *m*) Received amplitudes $|S_{21}|$ (purple lines) and $|S_{31}|$ (cyan lines) in (c),(e),(g),(i) at $R = 2$ *m*. Thick dashed-dotted lines and thin solid lines correspond to the coil 1 inclined case and no inclined case as the reference in (b)-(i).

C. ROBUSTNESS

Our system has a feature of the robustness, which comes from the ratio of the two received wave amplitudes, i.e., even when each received wave amplitude is similarly deviated, the ratio of the wave amplitudes provides relatively stable performance. Below, we discuss the effects of conductor loss

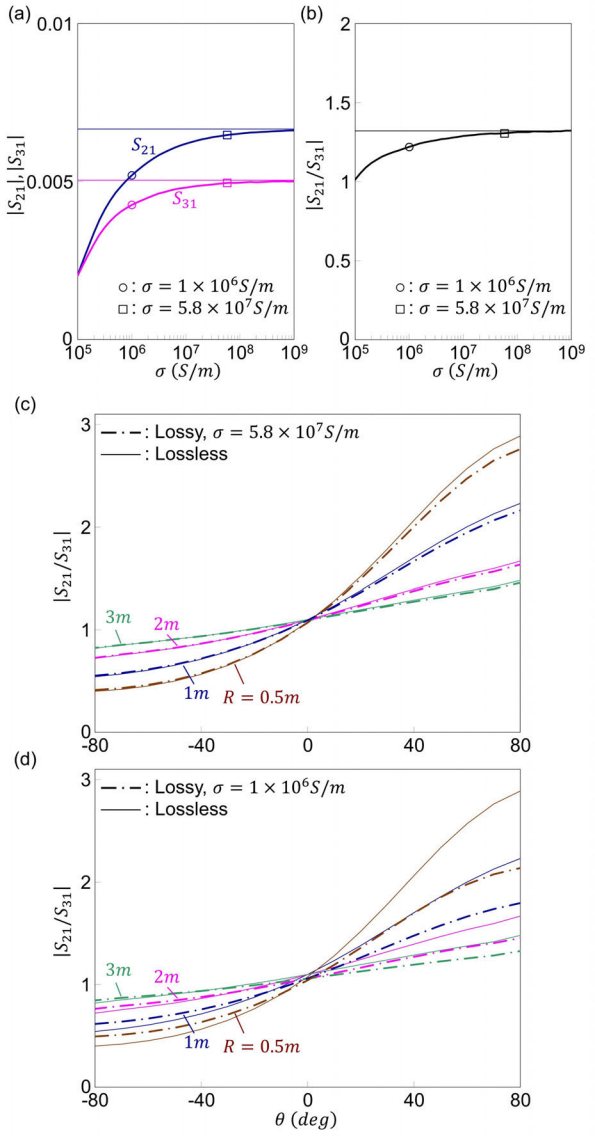

FIGURE 7. Effect of conductor loss of coil wires on the position sensing performance in the system of Fig. 1(a). (a) Received wave amplitudes $|S_{21}|$ (thick blue line), $|S_{31}|$ (thick pink line), and (b) the ratio $|S_{21}/S_{31}|$ at 10 *MHz* as a function of the conductivity σ of coil wires when coil 1 is positioned at $R = 2$ *m* and $\theta = 30°$. The squares and the circles represent values at $\sigma_c = 5.8 \times 10^7$ *S/m* for copper conductivity and $\sigma = 1 \times 10^6$ *S/m* for a heavily lossy material ($\sigma = \sigma_c/58$), respectively. (c),(d) Position sensing performance for $\sigma_c = 5.8 \times 10^7$ *S/m* in (c) and $\sigma = 1 \times 10^6$ *S/m* in (d) at 10 *MHz*. (brown lines: $R = 0.5$ *m*, blue lines: $R = 1$ *m*, pink lines: $R = 2$ *m*, green lines: $R = 3$ *m*) Thin lines correspond to the lossless case [Fig. 3(a)].

of wires and the placement of a ground plane near the coils on the system performance, respectively, as an internal and external deviation factors.

A typical case with a coil 1 position of $R = 2$ *m* and $\theta = 30°$ and a frequency of 10 *MHz* is considered to investigate the effect of conductor loss of coil wires. As shown in Fig. 7(a), both received wave amplitudes $|S_{21}|$ (thick blue line) and $|S_{31}|$ (thick pink line) decrease as wires become lossy (decrease of the conductivity σ). Thus, the ratio $|S_{21}/S_{31}|$ has a relatively small change, as shown in Fig. 7(b). Then, the ratio $|S_{21}/S_{31}|$ is obtained at 10 *MHz* as a function of angle θ for $R = 0.5$ *m* (brown lines), 1 *m* (blue lines), 2 *m* (pink lines), and 3 *m* (green lines) with two conductivity values, i.e., assuming copper with a conductivity of $\sigma_c = 5.8 \times 10^7$ *S/m* for Fig. 7(c) and a heavily lossy material with $\sigma = 1 \times 10^6$ *S/m* ($= \sigma_c/58$) for Fig. 7(d), respectively. Thick dashed-dotted lines correspond to the loss-included results and thin solid lines correspond to the lossless results for comparison, which were shown in Fig. 3(a). Although both of $|S_{21}|$ and $|S_{31}|$ are reduced due to the conductivity loss, the ratio $|S_{21}/S_{31}|$ persists the position sensing capability for the two cases. This is understood from Eq. (4) that the loss rates γ_{20} and γ_{30}, which correspond to the conductor loss of coils 2 and 3, are included in the denominator and the numerator, respectively, in the ratio of the received wave amplitudes.

Next, a 1 $m \times 1$ *m* ground plane is placed at a distance D away from the bottom of the receiving coils in the system of Fig. 1(a) [Fig. 8(a)]. Likewise, the typical case with a coil 1 position of $R = 2$ *m* and $\theta = 30°$, and a frequency of 10 *MHz* is considered. It is observed in Fig. 8(b) that both received wave amplitudes $|S_{21}|$ (thick blue line) and $|S_{31}|$ (thick pink line) are similarly deviated, i.e., as the ground plane gets closer to the receiving coils from $D = 2$ *m* to 5 *cm*, $|S_{21}|$ and $|S_{31}|$ have smaller values with respect to the case without the ground plane (horizontal blue and pink lines), and then steeply go up when $D < 20$ *cm* for $|S_{21}|$ and $D < 25$ *cm* for $|S_{31}|$. Due to the similar deviation, the ratio $|S_{21}/S_{31}|$ exhibits a relatively small change [Fig. 8(c)] as a function of D comparing with each change of $|S_{21}|$ and $|S_{31}|$. The similar deviation is seen in the spectra of $|S_{21}|$ (thick blue dashed-dotted line) and $|S_{31}|$ (thick pink dashed-dotted line) in Fig. 8(d) for $D = 10$ *cm* and in Fig. 8(e) for $D = 5$ *cm*, i.e., the frequencies at the peaks are shifted-down for both $|S_{21}|$ and $|S_{31}|$. As expected from the observations, the position sensing capability still exists (thick dashed-dotted lines) when the ground plane is placed at $D = 10$ *cm* [Fig. 8(f)] and $D = 5$ *cm* [Fig. 8(g)] although the sensitivity is degraded. The ratio $|S_{21}/S_{31}|$ has almost flat lines when the ground plane is placed at $D = 2$ *cm*, where the Fano resonance phenomenon disappears, and each of $|S_{21}|$ and $|S_{31}|$ has a single resonance peak around the intrinsic resonance frequency of 10 *MHz*.

We discuss possible application scenarios of our position sensing scheme. For noise sensing applications, our sensing scheme is applicable when the frequency of a dominant noise source is known such as switching noise of power converters [42]. Tunable impedance-matching techniques were well established for magnetic coils [13]–[15], which may allow the adjustment of resonance frequencies of the coils by a few tens of percentage. In addition, our position sensing scheme may be used as an add-on for a wireless power transfer system, i.e., power is wirelessly transferred from coil 1 to coil 4, and the pair of coils 2 and 3 is implemented off the side for sensing the position of coil 1. The pair of coils 2 and 3, or coil 4 is switched on when sensing the position of coil 1 or receiving power from coil 1.

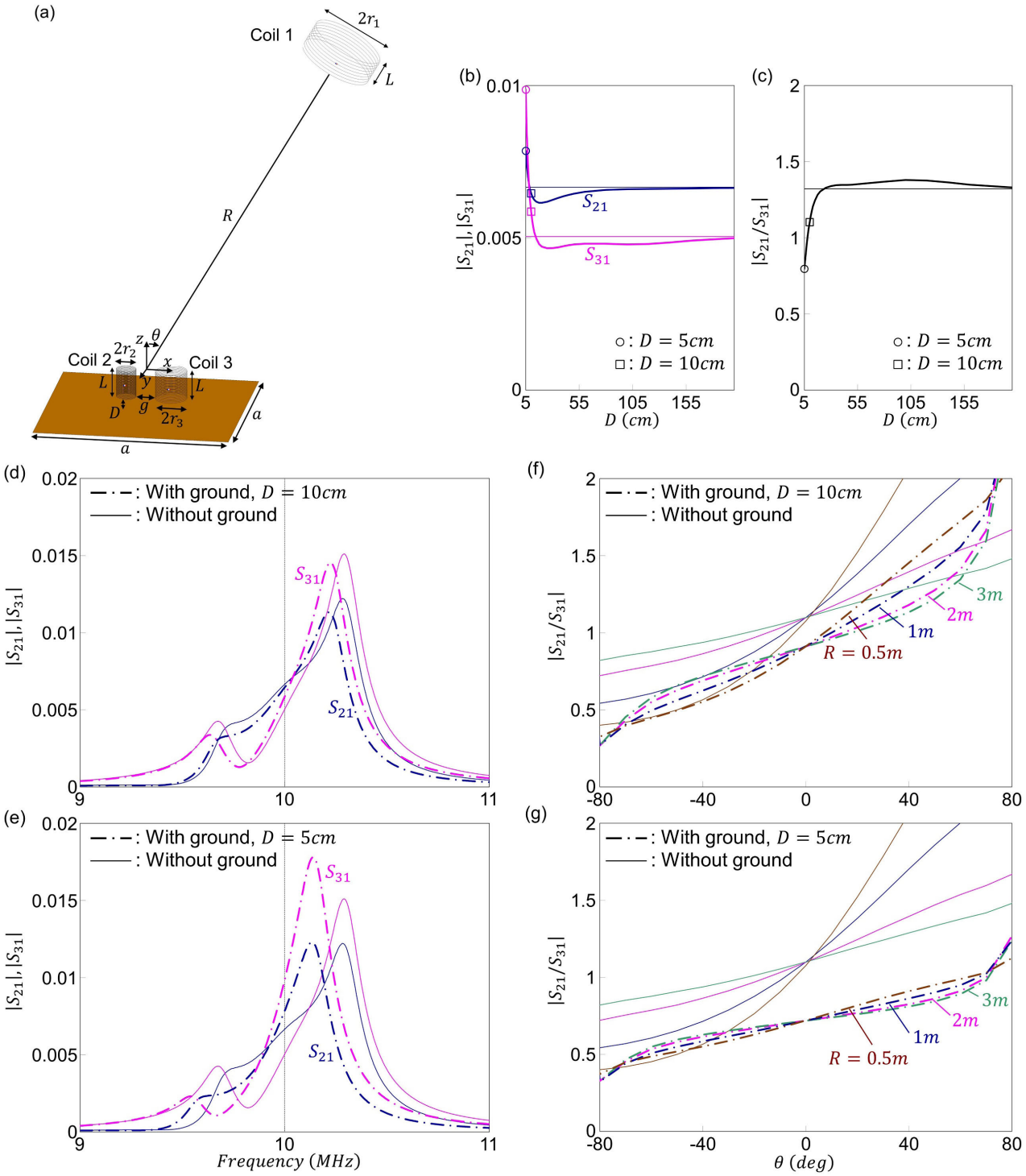

FIGURE 8. (a) Geometry of the system of Fig. 1(a), where a square ground plane with $a = 1$ *m* is placed at $z = -D - L$. (b) Received wave amplitudes $|S_{21}|$ (thick blue line), $|S_{31}|$ (thick pink line), and (c) the ratio $|S_{21}/S_{31}|$ at 10 *MHz* as a function of the distance *D* when coil 1 is positioned at $R = 2$ *m* and $\theta = 30°$. The circles and the squares represent values at $D = 5$ *cm* and $D = 10$ *cm* in (b) and (c). (d),(e) Spectra of $|S_{21}|$ (thick blue dashed-dotted lines) and $|S_{31}|$ (thick pink dashed-dotted lines) for $D = 10$ *cm* in (d) and $D = 5$ *cm* in (e). (f),(g) Position sensing performance for $D = 10$ *cm* in (f) and $D = 5$ *cm* in (g) at 10 *MHz*. (brown lines: $R = 0.5$ *m*, blue lines: $R = 1$ *m*, pink lines: $R = 2$ *m*, green lines: $R = 3$ *m*) Thin lines correspond to the case without the ground plane in (b)-(g).

IV. CONCLUSION

We have shown that the position sensing of a transmitting coil is possible by comparing wave amplitudes in a pair of two receiving coils and its angular derivative in a Fano resonance phenomenon. A coupled mode theory has been developed to elucidate how coupling strengths among coils are linked to

the ratio of the received wave amplitudes. Our results point to a midrange position sensing mechanism in the kilohertz-megahertz range.

The angular derivative of the ratio of received wave amplitudes is obtained by mechanical rotation of the pair of receiving coils, which allows position sensing in static systems. Our challenge is to tackle position sensing in dynamic systems without such mechanical rotation.

REFERENCES

[1] A. Kurs, A. Karalis, R. Moffatt, J. D. Joannopoulos, P. Fisher, and M. Soljačić, "Wireless power transfer via strongly coupled magnetic resonances," *Science*, vol. 317, no. 5834, pp. 83–86, Jul. 2007.

[2] A. Karalis, J. D. Joannopoulos, and M. Soljačić, "Efficient wireless non-radiative mid-range energy transfer," *Ann. Phys.*, vol. 323, no. 1, pp. 34–48, Jan. 2008.

[3] T. Imura and Y. Hori, "Maximizing air gap and efficiency of magnetic resonant coupling for wireless power transfer using equivalent circuit and Neumann formula," *IEEE Trans. Ind. Electron.*, vol. 58, no. 10, pp. 4746–4752, Oct. 2011.

[4] X. Yu, S. Sandhu, S. Beiker, R. Sassoon, and S. Fan, "Wireless energy transfer with the presence of metallic planes," *Appl. Phys. Lett.*, vol. 99, no. 21, pp. 214102:1–214102:3, Nov. 2011.

[5] S. Y. R. Hui, W. Zhong, and C. K. Lee, "A critical review of recent progress in mid-range wireless power transfer," *IEEE Trans. Power Electron.*, vol. 29, no. 9, pp. 4500–4511, Sep. 2014.

[6] J. Kim, H.-C. Son, K.-H. Kim, and Y.-J. Park, "Efficiency analysis of magnetic resonance wireless power transfer with intermediate resonant coil," *IEEE Antennas Wireless Propag. Lett.*, vol. 10, pp. 389–392, May 2011.

[7] S. Cheon, Y.-H. Kim, S.-Y. Kang, M. L. Lee, J.-M. Lee, and T. Zyung, "Circuit-model-based analysis of a wireless energy-transfer system via coupled magnetic resonances," *IEEE Trans. Ind. Electron.*, vol. 58, no. 7, pp. 2906–2914, Jul. 2011.

[8] Y. Tak, J. Park, and S. Nam, "Mode-based analysis of resonant characteristics for near-field coupled small antennas," *IEEE Antennas Wireless Propag. Lett.*, vol. 8, pp. 1238–1241, Nov. 2009.

[9] C.-J. Chen, T.-H. Chu, C.-L. Lin, and Z.-C. Jou, "A study of loosely coupled coils for wireless power transfer," *IEEE Trans. Circuits Syst. II, Exp. Briefs*, vol. 57, no. 7, pp. 536–540, Jul. 2010.

[10] E. M. Thomas, J. D. Heebl, C. Pfeiffer, and A. Grbic, "A power link study of wireless non-radiative power transfer systems using resonant shielded loops," *IEEE Trans. Circuits Syst. I, Reg. Papers*, vol. 59, no. 9, pp. 2125–2136, Sep. 2012.

[11] J. Park, Y. Tak, Y. Kim, Y. Kim, and S. Nam, "Investigation of adaptive matching methods for near-field wireless power transfer," *IEEE Trans. Antennas Propag.*, vol. 59, no. 5, pp. 1769–1773, May 2011.

[12] A. P. Sample, D. A. Meyer, and J. R. Smith, "Analysis, experimental results, and range adaptation of magnetically coupled resonators for wireless power transfer," *IEEE Trans. Ind. Electron.*, vol. 58, no. 2, pp. 544–554, Feb. 2011.

[13] T. C. Beh, M. Kato, T. Imura, S. Oh, and Y. Hori, "Automated impedance matching system for robust wireless power transfer via magnetic resonance coupling," *IEEE Trans. Ind. Electron.*, vol. 60, no. 9, pp. 3689–3698, Sep. 2013.

[14] K. Sasaki, S. Sugiura, and H. Iizuka, "Distance adaptation method for magnetic resonance coupling between variable capacitor-loaded parallel-wire coils," *IEEE Trans. Microw. Theory Techn.*, vol. 62, no. 4, pp. 892–900, Apr. 2014.

[15] J. Kim and J. Jeong, "Range-adaptive wireless power transfer using multiloop and tunable matching techniques," *IEEE Trans. Ind. Electron.*, vol. 62, no. 10, pp. 6233–6241, Oct. 2015.

[16] S. Assawaworrarit, X. Yu, and S. Fan, "Robust wireless power transfer using a nonlinear parity-time-symmetric circuit," *Nature*, vol. 546, pp. 387–390, Jun. 2017.

[17] J. Kim, H.-C. Son, D.-H. Kim, and Y.-J. Park, "Optimal design of a wireless power transfer system with multiple self-resonators for an LED TV," *IEEE Trans. Consum. Electron.*, vol. 58, no. 3, pp. 775–780, Aug. 2012.

[18] J. Kim, J. Kim, S. Kong, H. Kim, I.-S. Suh, N. P. Suh, D.-H. Cho, J. Kim, and S. Ahn, "Coil design and shielding methods for a magnetic resonant wireless power transfer system," *Proc. IEEE*, vol. 101, no. 6, pp. 1332–1342, Jun. 2013.

[19] J. Shin, S. Shin, Y. Kim, S. Ahn, S. Lee, G. Jung, S.-J. Jeon, and D.-H. Cho, "Design and implementation of shaped magnetic-resonance-based wireless power transfer system for roadway-powered moving electric vehicles," *IEEE Trans. Ind. Electron.*, vol. 61, no. 3, pp. 1179–1192, Mar. 2014.

[20] S. Li and C. Chris Mi, "Wireless power transfer for electric vehicle applications," *IEEE J. Emerg. Sel. Topics Power Electron.*, vol. 3, no. 1, pp. 4–17, Mar. 2015.

[21] S. Y. Choi, B. W. Gu, S. Y. Jeong, and C. T. Rim, "Advances in wireless power transfer systems for roadway-powered electric vehicles," *IEEE J. Emerg. Sel. Topics Power Electron.*, vol. 3, no. 1, pp. 18–36, Mar. 2015.

[22] Z. Zhang, H. Pang, A. Georgiadis, and C. Cecati, "Wireless power transfer—An overview," *IEEE Trans. Ind. Electron.*, vol. 66, no. 2, pp. 1044–1058, Feb. 2019.

[23] J. S. Ho, S. Kim, and A. S. Y. Poon, "Midfield wireless powering for implantable systems," *Proc. IEEE*, vol. 101, no. 6, pp. 1369–1378, Jun. 2013.

[24] A. Ibrahim and M. Kiani, "A figure-of-merit for design and optimization of inductive power transmission links for millimeter-sized biomedical implants," *IEEE Trans. Biomed. Circuits Syst.*, vol. 10, no. 6, pp. 1100–1111, Dec. 2016.

[25] M. R. Basar, M. Y. Ahmad, J. Cho, and F. Ibrahim, "Stable and high-efficiency wireless power transfer system for robotic capsule using a modified Helmholtz coil," *IEEE Trans. Ind. Electron.*, vol. 64, no. 2, pp. 1113–1122, Feb. 2017.

[26] S. Nakamura, R. Koma, and H. Hashimoto, "Efficient wireless power transmission based on position sensing using magnetic resonance coupling," *SICE J. Control, Meas., Syst. Integr.*, vol. 5, no. 3, pp. 153–161, 2012.

[27] J. C. Chen, R. E. Hudson, and K. Yao, "Maximum-likelihood source localization and unknown sensor location estimation for wideband signals in the near-field," *IEEE Trans. Signal Process.*, vol. 50, no. 8, pp. 1843–1854, Aug. 2002.

[28] U. Paoletti, "Direction finding techniques in reactive near field of impulsive electromagnetic noise source aiming at pantograph arcing localization," *IEEE Sensors J.*, vol. 19, no. 11, pp. 4193–4200, Jun. 2019.

[29] I. Echeverria, F. Arteche, M. Iglesias, A. Pradas, J. Piedrafita, and F. J. Arcega, "Common mode noise propagation and effects in a four-wheel drive electric vehicle," *IEEE Trans. Electromagn. Compat.*, vol. 60, no. 1, pp. 132–139, Feb. 2018.

[30] U. Fano, "Effects of configuration interaction on intensities and phase shifts," *Phys. Rev.*, vol. 124, no. 6, pp. 1866–1878, Dec. 1961.

[31] S. Fan, W. Suh, and J. D. Joannopoulos, "Temporal coupled-mode theory for the Fano resonance in optical resonators," *J. Opt. Soc. Amer. A, Opt. Image Sci.*, vol. 20, no. 3, pp. 569–572, Mar. 2003.

[32] A. E. Miroshnichenko, S. Flach, and Y. S. Kivshar, "Fano resonances in nanoscale structures," *Rev. Modern Phys.*, vol. 82, no. 3, pp. 2257–2298, Aug. 2010.

[33] B. Luk'yanchuk, N. I. Zheludev, S. A. Maier, N. J. Halas, P. Nordlander, H. Giessen, and C. T. Chong, "The fano resonance in plasmonic nanostructures and metamaterials," *Nature Mater.*, vol. 9, no. 9, pp. 707–715, Sep. 2010.

[34] S. Yi, M. Zhou, Z. Yu, P. Fan, N. Behdad, D. Lin, K. X. Wang, S. Fan, and M. Brongersma, "Subwavelength angle-sensing photodetectors inspired by directional hearing in small animals," *Nature Nanotechnol.*, vol. 13, no. 12, pp. 1143–1147, Dec. 2018.

[35] T. Lee, T. Nomura, X. Su, and H. Iizuka, "Fano-like acoustic resonance for subwavelength directional sensing: 0-360 degree measurement," *Adv. Sci.*, vol. 7, no. 6, pp. 1903101:1–1903101:9, Mar. 2020.

[36] B. L. Cannon, J. F. Hoburg, D. D. Stancil, and S. C. Goldstein, "Magnetic resonant coupling as a potential means for wireless power transfer to multiple small receivers," *IEEE Trans. Power Electron.*, vol. 24, no. 7, pp. 1819–1825, Jul. 2009.

[37] A. Kurs, R. Moffatt, and M. Soljačić, "Simultaneous mid-range power transfer to multiple devices," *Appl. Phys. Lett.*, vol. 96, no. 4, Jan. 2010, Art. no. 044102.

[38] D. Ahn and S. Hong, "Effect of coupling between multiple transmitters or multiple receivers on wireless power transfer," *IEEE Trans. Ind. Electron.*, vol. 60, no. 7, pp. 2602–2613, Jul. 2013.

[39] H. A. Haus, *Waves and Fields in Optoelectronics*. Englewood Cliffs, NJ, USA: Prentice-Hall, 1984.

[40] X. Yu, T. Skauli, B. Skauli, S. Sandhu, P. B. Catrysse, and S. Fan, "Wireless power transfer in the presence of metallic plates: Experimental results," *AIP Adv.*, vol. 3, no. 6, Jun. 2013, Art. no. 062102.
[41] *Altair FEKO User Guide, 2019.1.1*, Altair Eng., Troy, MI, USA, 2019.
[42] T. Liu, T. T. Y. Wong, and Z. John Shen, "A survey on switching oscillations in power converters," *IEEE J. Emerg. Sel. Topics Power Electron.*, vol. 8, no. 1, pp. 893–908, Mar. 2020.

TAEHWA LEE (Member, IEEE) received the B.S. degree from Hanyang University, Seoul, South Korea, in 2007, the M.S. degree from POSTECH, Pohang, South Korea, in 2009, and the Ph.D. degree from the University of Michigan, Ann Arbor, MI, USA, in 2015, all in mechanical engineering. Before moving to USA, he was the Assistant Manager of Samsung Heavy Industry, Inc., South Korea, from 2009 to 2011. After completing his Ph.D. degree, he was a Postdoctoral Research Associate with Stanford University, from 2016 to 2017. In 2017, he joined the Toyota Research Institute of North America, Toyota Motor North America, Inc., Ann Arbor. His research interests include wave-matter interaction in electromagnetics and acoustics.

DANIEL HASHEMI received the M.S. degree in physics from the K. N. T. University of Technology, Tehran, Iran, in 2005, and the Ph.D. degree in physics from the International Max Planck Research School for Science and Technology of Nanostructures in conjunction with Martin Luther University, Halle, Germany, in 2015. After receiving his Ph.D. degree, he was a Postdoctoral Fellow and an Adjunct Faculty with the University of Michigan, Ann Arbor, USA, from 2016 to 2017. He continued his research journey at the Air Force Research Laboratory, Wright-Patterson Air Force Base, USA, from 2017 to 2019. In 2019, he joined the Toyota Research Institute of North America, Ann Arbor, USA. His current research interests include the discovery of topological systems and high-performance batteries.

KENICHI YATSUGI received the M.S. degree in applied physics from Osaka University, Osaka, Japan, in 2012. He joined Toyota Central Research and Development Laboratories, Inc., in 2012. His current research interest includes developments of electromagnetic devices for automotive applications. He is a member of the Japan Society of Applied Physics (JSAP).

MICHIO YASUNISHI received the B.S. degree in nuclear engineering and the M.S. and D.S. degrees in electromagnetic engineering from Osaka University, Osaka, Japan, in 1998, 2000, and 2004, respectively. He was with Toyota Communication Systems Company Ltd., Nagoya, Japan, from 2004 to 2006, and Toyota Technical Development Corporation Ltd., Toyota, Japan, from 2006 to 2015. He joined Toyota Motor Corporation Ltd., Toyota, in 2016. He is a member of the Japan Society of Applied Electromagnetics and Mechanics (JSAEM).

HIROSHI YOSHIMOTO received the M.S. degree in mechanical engineering from Sophia University, Tokyo, Japan, in 1995. He has more than 20 years' experience in the automotive industry. He joined Toyota Motor Corporation Ltd., Toyota, Japan, in 2016. He is a member of the Society of Automotive Engineers of Japan (JSAE).

HIDEO IIZUKA (Member, IEEE) received the B.S. and M.S. degrees in electrical engineering from Saitama University, Saitama, Japan, in 1995 and 1997, respectively, and the Ph.D. degree in engineering from the Nagoya Institute of Technology, Nagoya, Japan, in 2007. In 1997, he joined Toyota Central Research and Development Laboratories Inc., Nagakute, Japan. From 2001 to 2002, he was a Visiting Scholar with the University of Birmingham, Birmingham, U.K. From 2008 to 2011, he was with the Toyota Research Institute of North America, Toyota Motor North America, Inc., Ann Arbor, MI, USA, where he has been since 2017. His research interests include analyses and developments of devices and sub-systems in electromagnetics and acoustics.